Sound & Vibration 2026, 60(5), 4497.
doi: https://doi.org/10.59400/sv4497

Article

Broadband vibration suppression of a nonlinear beam using a fractional-order inerter-assisted tuned mass damper

Yogeesh Nijalingappa[1,2,3*], Suleiman Ibrahim Mohammad[1,4], Tarun Madan Kanade[5], Asokan Vasudevan[3], P. William[6,7], Mohammad Faleh Ahmmad Hunitie[8]

[1] Department of Mathematics, Government First Grade College, Tumakuru 572102, India
[2] Mathematics & Natural Sciences, Gulf University for Science & Technology, Safat 13060, Kuwait
[3] Faculty of Business and Communications, INTI International University, Nilai 71800, Malaysia
[4] Department of Business Administration, Business School, Al al-Bayt University, Mafraq 25113, Jordan
[5] Symbiosis Institute of Operations Management, Symbiosis International (Deemed University), Nashik 422008, India
[6] School of Computer Science and Technology, Karunya Institute of Technology and Sciences (Deemed University), Coimbatore 641114, India
[7] Centre for Research and Consultancy, UNITAR International University, Kelana Jaya 47301, Malaysia
[8] Department of Public Administration, School of Business, University of Jordan, Amman 11942, Jordan
*** Corresponding author:** Yogeesh Nijalingappa, yogeesh.r@gmail.com

CITATION

Nijalingappa Y, Mohammad SI, Kanade TM. Broadband vibration suppression of a nonlinear beam using a fractional-order inerter-assisted tuned mass damper. Sound & Vibration. 2026; 60(5): 4497. https://doi.org/10.59400/sv4497

ARTICLE INFO

Received: 10 June 2026
Revised: 4 July 2026
Accepted: 10 July 2026
Available online: 24 July 2026

Abstract: This study presents an analytical method for reducing broadband vibration in a simply supported nonlinear beam fitted with an inerter-assisted tuned mass damper. The first bending mode is obtained by Galerkin projection, geometric nonlinearity is represented by a cubic stiffness term, and beam damping is described by a fractional-order derivative. A single-harmonic balance formulation converts the coupled equations into an amplitude-dependent cubic equation that is solved directly over the forcing-frequency range. The absorber is optimized with respect to inertance ratio, tuning ratio, damping ratio, and fractional order. The objective is to minimize the largest beam amplitude between 7 and 14 Hz. For the beam considered, increasing the inertance ratio from 0 to 0.20 raises the peak-response reduction from about 4.5% to about 52%, while the physical absorber mass ratio remains 0.04. The optimal tuning ratio decreases as inertance increases, whereas the required absorber damping generally increases. A ±5% stiffness study shows that the optimized designs remain effective under moderate uncertainty. The results also clarify how fractional damping modifies the balance between effective stiffness and dissipation, enabling the proposed maps to support robust initial absorber selection before detailed high-fidelity validation. The resulting design maps and regression equations provide useful preliminary settings for later finite-element or experimental verification.

Keywords: beam vibration; inerter-assisted tuned mass damper; fractional damping; harmonic balance; nonlinear dynamics; passive control; design map

1. Introduction

Passive vibration control is widely used because it is simple, reliable, and easy to apply in machines, civil structures, and lightweight mechanical systems. Within this area, the inerter has become especially important after Smith introduced it as the missing two-terminal mechanical element relating terminal force to relative acceleration [1]. Once the concept entered structural vibration mitigation, a large body of work showed that inertance can amplify the dynamic effect of a relatively small, attached mass and therefore improve absorber performance without the severe space penalty associated with purely mass-based devices [2–6]. Later developments addressed long-span bridges [7], wind-excited flexible structures [8], generalized optimal structural models [9], wind-excited tall buildings [10], fractional beam dynamics [11], wind-turbine blades [12], and seismic, bridge, base-isolated, and enhanced structural-control systems [13–18]. Related work examined nonlinear tuned mass damping [19], fractional beam and flexible-structure models [20–22], recent inerter-based structural control [23, 24], and fractional-order vibration formulations [25–30]. Together, these streams identify a still relatively unexplored design space: inerter-assisted vibration absorbers connected to flexible members whose damping is described more accurately by fractional calculus than by classical proportional damping.

Two practical difficulties must be considered. First, lightly damped beams under harmonic loading rarely remain strictly linear when the response grows to serviceability-relevant amplitudes. Stretching-induced mid-plane effects, even when mild, produce amplitude-dependent detuning and hardening behavior that shifts resonance and degrades narrow-band absorber settings. Second, fractional damping modifies both the real and imaginary parts of dynamic stiffness in a frequency-dependent manner, so the “best” absorber tuning can no longer be inferred reliably from undamped or viscously damped formulas alone. In spite of the large literature on tuned mass dampers, inerter-assisted absorbers, and fractional beams, most published studies treat either a linear host with advanced absorber design or a fractional host without a detailed inertance-oriented design map. That leaves a useful analytical gap for a submission to a journal oriented toward sound, vibration, dynamic analysis, and practically relevant numerical design.

To be more specific, while almost all previous studies focus on one of the three aspects above, comparatively few studies incorporate them into one parametric design platform. The primary novelty of this work comprises the combined formulation and directly computed design maps.

The present paper addresses this gap through an analytically explicit study of a simply supported steel beam fitted with an inerter-assisted tuned mass damper at midspan. The host beam is a first-mode reduction that applies to appropriate excitation bands when they are both concentrated around the first bending resonance and tuned to the dominant band of the absorber. The standard cubic stiffness term originating from the extensional stretching of a slander beam is included by means of geometric nonlinearity. The fractional derivative of order $\alpha \in (0, 1]$ and the structural damping case justify that it encompasses classical viscous behavior ($\alpha = 1$) and sub-viscous cases with accentuated frequency dependence [20, 22, 30]. The appended device is simply modeled as a secondary oscillator with its effective inertia increased through the presence of an inerter. This results in a fractional, coupled system that is compact but physically meaningful and non-linear.

You perform explicit calculations and reproducible numerical comparisons. The reduced equations are then obtained, and the harmonic-balance amplitude polynomial is subsequently derived. The design space is next explored with respect to the inertance ratio β, tuning ratio η, absorber damping ratio ξ and fractional order α. The target is the maximum response magnitude in the 7–14 Hz forcing band. Along with the uncertainty in material properties, boundary restraint, and modal reduction, a ±5% stiffness perturbation is also assumed.

It makes four main contributions. First, it provides a full first-mode derivation for an inertially nonlinear beam with fractional damping and inerter assistance. Second, it represents the harmonic-balance response as a cubic polynomial in a^2 so that through algebraic manipulation all steady-state solutions are obtained without time marching. Third, it provides numerical design maps and measured trends through parameter tuning, damping, and inertance. To develop simple regression relations and stiffness-perturbation checks for preliminary engineering design.

2. Physical model and modal reduction

2.1. Beam kinematics and governing equation

Let us consider a simply supported Euler–Bernoulli beam of length L, cross-sectional area A, second moment of area I, Young's modulus E, and material density ρ. Denote cylindrical transverse displacement as $w(x,t)$. Based on the standard assumptions of limited rotations, slender geometry, and 1st mode dominance, the exact model for the nonlinear beam with fractional damping controlled by an external concentrated force acting at $x_a = L/2$ can be expressed as:

$$\rho A\ddot{w} + c_\alpha^C D_t^\alpha w + EI w_{xxxx} + \frac{EA}{2L}\left(\int_0^L w_x^2 dx\right) w_{xx} = p(x,t) - \delta\left(x - x_a\right) f_c(t).$$

Where ${}^C D_t^\alpha(\cdot)$ is the Caputo-type fractional derivative of order α, $p(x,t)$ is the external loading distribution, and $f_c(t)$ is the interaction force transferred by the attached absorber. The nonlinearity stretching term is the normal low-order representation, which produces a cubic restoring contribution after modal projection. As both the forcing and the control device are located at midspan, the first flexural mode is a good representation of most of the dynamics.

The modelled frequencies obtained scale as n^2 for this 'simple' example of a uniform simply supported Euler-Bernoulli beam; thus, the second bending frequency is quadruple the first natural frequency, $f_2 \approx 4f_1 = 39.09$ Hz. No direct resonance of the second mode would be expected, as the investigated band ends at 14 Hz. This is why the first-mode approximation is suitable for the excitation and attachment configuration given, while a multimode model should be used when higher multi-modal harmonics are approached by any forcing in either position of attachment.

Assigning the first simply supported mode:

$$\phi_1(x) = \sin\left(\frac{\pi x}{L}\right),$$

and the approximation:

$$w(x,t) \approx \phi_1(x) q(t).$$

Galerkin projection yields the generalized equation:

$$M\ddot{q} + c_p\, {}^{C}D_t^{\alpha} q + Kq + K_3 q^3 + f_c = F_0 \cos \Omega t.$$

The generalized coefficients are:

$$\begin{gathered} M = \rho A \int_0^L \phi_1^2 dx = \tfrac{\rho A L}{2},\ K = EI \int_0^L \phi_{1,xx}^2 dx = \tfrac{EI\pi^4}{2L^3} \\ K_3 = \tfrac{EA}{2L} \left(\int_0^L \phi_{1,x}^2 dx \right)^2 = \tfrac{EA\pi^4}{8L^3} \end{gathered}.$$

F_0 is the first generalized component of the applied load, which represents the forcing amplitude. The calculation approach for the present beam is summarized in **Table 1**, which results in a linearized natural frequency:

$$\omega_1 = \sqrt{\frac{K}{M}},\ f_1 = \frac{\omega_1}{2\pi} = 9.7722 \text{ Hz},$$

this is an indication of hardening of the host—since the cubic stiffness coefficient is positive—so when increasing forcing amplitudes, we expect the resonance peak to move also towards f_1.

Table 1. Beam, loading, and search parameters used in the nonlinear fractional vibration study.

Parameter	Symbol	Value
Beam length	L	1.20 m
Beam width	b_w	40 mm
Beam thickness	h	6 mm
Young's modulus	E	210 GPa
Density	ρ	7,850 kg/m^3
Cross-sectional area	A	0.000240 m^2
Second moment of area	I	7.2000×10^{-10} m^4
Generalized modal mass	M	1.1304 kg
Generalized linear stiffness	K	4,261.65 N/m
Generalized cubic stiffness	K_3	3.5514×10^8 N/m^3
Linearized first natural frequency	f_1	9.7722 Hz
Forcing amplitude	F_0	4 N
Physical absorber mass ratio	μ	0.04
Target equivalent modal damping	ζ_p	0.012
Search range of tuning ratio	η	0.78–1.10
Search range of absorber damping ratio	ξ	0.04–0.26

2.2. Fractional damping representation

For the coefficients of this model to be practically interpretable, the fractional damping coefficient is associated with a target equivalent damping ratio ζ_p at the fundamental frequency. When the fractional term is written in the frequency domain by $c_p(i\Omega)^{\alpha}$, then at $\Omega = \omega_1$, this means that the imaginary part of the complex stiffness is according to $c_p \omega_1^{\alpha} \sin(\alpha\pi/2)$ [2]. By matching the loss, which contributes to the viscous reference $2\zeta_p M \omega_1$ gives:

$$c_p = \frac{2\zeta_p M \omega_1^{2-\alpha}}{\sin(\alpha\pi/2)}.$$

This definition appears attractive because it keeps a similar damping level at the design frequency, while allowing off-resonant frequency dependence to vary with α. The coefficients presented here can be found in **Table 2**. As α decreases from 1.0 to 0.6, the required coefficient c_p rises sharply, but the effective dissipation is redistributed over frequency rather than acting like classical viscous damping. That redistribution plays an important role in the optimization results later in the paper.

Table 2. Fractional damping coefficients derived from the equivalent damping-ratio matching relation, the last column lists the uncontrolled peak values used as the baseline for percentage reduction.

Fractional order α	Equivalent modal coefficient c_p	Uncontrolled peak amplitude (mm)
1.0	1.6658	4.488
0.8	3.9907	4.471
0.6	10.6888	4.453

The matching condition is local to ω_1. For $\alpha < 1$, the term $c_p(i\Omega)^\alpha$ contains both a storage component, $c_p\Omega^\alpha \cos\left(\frac{\pi\alpha}{2}\right)$, and a loss component, $c_p\Omega^\alpha \sin\left(\frac{\pi\alpha}{2}\right)$. Consequently, the increase of c_p from 1.6658 to 10.6888 is not merely a change in damping magnitude; it also changes the apparent dynamic stiffness away from ω_1. Thus, a broadband identification that reduces the error in both storage and loss moduli at 7–14 Hz could lead to somewhat different optimal η and ξ. We keep the present single-frequency matching as a transparent reference calibration and emphasize that the parameters determined this way should be re-identified when broad-band experimental damping data are available.

2.3. Inerter-assisted absorber model

The absorber is attached at midspan and consists of a physical auxiliary mass m_a, a spring of stiffness k_a, a damper with coefficient c_a, and an inerter that contributes inertance b to the secondary branch. Let $u_a(t)$ denote the absolute motion of the absorber mass. For the topology considered here, the device equations are written as:

$$
\begin{gathered}
M\ddot{q} + c_p\, {}^{C}D_t^{\alpha} q + Kq + K_3 q^3 + c_a\left(\dot{q} - \dot{u}_a\right) + k_a\left(q - u_a\right) = F_0 \cos\Omega t, \\
\left(m_a + b\right)\ddot{u}_a + c_a\left(\dot{u}_a - \dot{q}\right) + k_a\left(u_a - q\right) = 0.
\end{gathered}
$$

The inertance therefore augments the effective inertia of the secondary oscillator without increasing the carried dead mass by the same amount. For parametric analysis, it is convenient to introduce:

$$
\begin{gathered}
\mu = \frac{m_a}{M},\ \beta = \frac{b}{M},\ m_t = m_a + b = M(\mu + \beta), \\
\omega_a = \sqrt{\frac{k_a}{m_t}},\ \eta = \frac{\omega_a}{\omega_1},\ \xi = \frac{c_a}{2 m_t \omega_a}.
\end{gathered}
$$

The absorber is thus parameterized by a physical mass ratio μ, inertance ratio β, tuning ratio η, and damping ratio ξ. In the present study, μ is fixed at 0.04, and the design variables are β, η, and ξ. This choice isolates the effect of inertance on the tuning landscape while keeping the added physical mass modest.

3. Single-harmonic balance and effective dynamic stiffness

3.1. Complex-amplitude formulation

To obtain steady-state frequency-response relations without long time-domain integration, the coupled system is approximated by its dominant harmonic content. Let,

$$q(t) \approx \Re\left\{Qe^{i\Omega t}\right\},\ u_a(t) \approx \Re\left\{Ue^{i\Omega t}\right\},$$

where Q and U are complex amplitudes. The cubic restoring force is replaced by its first-harmonic equivalent,

$$q^3(t) \approx \frac{3}{4}|Q|^2\Re\left\{Qe^{i\Omega t}\right\},$$

which is standard for a weakly to moderately nonlinear hardening oscillator.

The cubic identity $q^3 = (3/4)a^3\cos(\Omega t) + (1/4)a^3\cos(3\Omega t)$ shows explicitly that the retained fundamental term is accompanied by an omitted third harmonic. The uncontrolled peaks in **Table 2** are 4.453–4.488 mm, not > 15 mm. Still, the single-harmonic solution should be treated as a first harmony backbone estimate close to possible jump regions. Higher-order harmonic balance or time-domain continuation is needed to accurately characterise third harmonic amplitudes and branch stability if 3Ω approaches a higher structural mode.

$$\begin{gathered}\left[-M\Omega^2 + K + \tfrac{3}{4}K_3|Q|^2 + c_p(i\Omega)^\alpha + k_a + i\Omega c_a\right]Q - (k_a + i\Omega c_a)\,U = F_0 \\ -(k_a + i\Omega c_a)\,Q + \left[-m_t\Omega^2 + k_a + i\Omega c_a\right]U = 0\end{gathered}.$$

Defining the coupling dynamic stiffness,

$$C_c = k_a + i\Omega c_a,$$

and the primary nonlinear dynamic stiffness,

$$D_p = -M\Omega^2 + K + \frac{3}{4}K_3|Q|^2 + c_p(i\Omega)^\alpha + C_c,$$

elimination of U gives a scalar effective stiffness relation,

$$\mathcal{D}_{\mathrm{eff}}(\Omega, |Q|)Q = F_0,\ \mathcal{D}_{\mathrm{eff}} = D_p - \frac{C_c^2}{C_c - m_t\Omega^2}.$$

Thus we must have the nonlinear algebraic condition for the steady-state amplitude $a = |Q|$:

$$a = \frac{F_0}{|\mathcal{D}_{\mathrm{eff}}(\Omega, a)|}.$$

The latter expression is at the heart of this paper: it combines the effects of beam nonlinearity, fractional damping, and inerter-assisted absorption into a single amplitude-dependent scalar equation. Given a computed over the frequency band, one finds by back-substituting its absorber amplitude and force.

3.2. Direct polynomial-root solution and branch selection

For numerical evaluation, the amplitude equation is squared and written in terms of $x = a^2$. If $H(\Omega)$ denotes the complex linear part of the effective stiffness and $c = 3K_3/4$, the governing polynomial is $c^2x^3 + 2c\,\mathrm{Re}[H]x^2 + |H|^2x - F_0^2 = 0$. Positive real roots are calculated at all frequencies, and a direct substitution results in a relative algebraic residual of less than 10^{-10}. A conservative design goal utilizes the largest allowable positive root, which avoids a branch-dependent fixed-point iteration that could inflate the reported peak.

$$a^{(r+1)} = \lambda a^{(r)} + (1-\lambda)\frac{F_0}{|\mathcal{D}_{\mathrm{eff}}(\Omega, a^{(r)})|},\ 0 < \lambda < 1.$$

Frequency continuation only sorts neighbouring roots into continuous response paths and does not create or eliminate algebraic solutions. All positive roots are maintained before the conservative maximum is applied if several positive roots occur. This process varies the multivalued parameter amplitudes for the first harmonic of the model, but does not by itself indicate a stable dynamical state. This makes it identifiable as an item not addressed in the present design-stage study because stability and jump-transition verification would require Floquet analysis or time-domain simulation.

3.3. Objective function and design space

The design objective is defined as the maximum steady-state beam amplitude over the forcing band $f \in [7, 14]$ Hz,

$$J(\beta, \eta, \xi, \alpha) = \max_{\Omega \in [2\pi\times 7, 2\pi\times 14]} a(\Omega; \beta, \eta, \xi, \alpha).$$

The absorber parameters are optimized over $\{1.0, 0.8, 0.6\}$ for each fractional order α and over $\{0, 0.05,\ 0.10,\ 0.15,\ 0.20\}$ for each inertance ratio β,

$$0.78 \le \eta \le 1.10,\ \ 0.04 \le \xi \le 0.26.$$

The limits are wide enough to encompass the classical tuned-mass-damper neighbourhood while allowing for the inertance-enhanced device to retune far below the primary frequency once effective inertia is large.

Since the target is specifically band-limited, an optimum for which the maximum response occurs at 7 or 14 Hz must be a boundary-active solution. This type of outcome may mean that attenuation has pushed a resonance out to or beyond the selected service band, but it is not eliminated overall. As such, the boundary cases in **Table 3**, and the $\beta = 0$ solutions at b14 Hz especially, are reported without having gained out-of-band optimality; design in practice should recast the sweep over an expanded frequency interval surrounding the service band.

Table 3. Optimums from grid search using the conservative positive-root harmonic-balance response from 7.0 to 14.0 Hz.

α	β	ηopt	ξopt	Controlled peak (m)	Reduction (%)	Peak frequency (Hz)
1.0	0.00	1.10	0.04	0.004287	4.48	14.00

Table 3. *Cont.*

α	β	ηopt	ξopt	Controlled peak (m)	Reduction (%)	Peak frequency (Hz)
1.0	0.05	1.10	0.22	0.003338	25.62	13.07
1.0	0.10	1.04	0.20	0.002530	43.63	9.28
1.0	0.15	0.96	0.26	0.002294	48.89	11.70
1.0	0.20	0.92	0.26	0.002168	51.69	8.20
0.8	0.00	1.10	0.04	0.004270	4.50	14.00
0.8	0.05	1.10	0.22	0.003427	23.36	13.25
0.8	0.10	1.04	0.20	0.002515	43.76	9.28
0.8	0.15	0.96	0.26	0.002311	48.32	11.78
0.8	0.20	0.92	0.26	0.002154	51.83	8.20
0.6	0.00	1.10	0.04	0.004252	4.52	14.00
0.6	0.05	1.10	0.24	0.003495	21.53	13.30
0.6	0.10	1.04	0.20	0.002496	43.94	9.28
0.6	0.15	0.98	0.24	0.002306	48.22	8.75
0.6	0.20	0.92	0.26	0.002136	52.03	8.20

4. Results: Uncontrolled and controlled frequency response

4.1. Baseline nonlinear response

The uncontrolled response was recomputed from the cubic amplitude polynomial to have an exact value before optimization. The first natural frequency linearized is 9.7722 Hz. Harmonic-balance peak ranges from 4.488 mm at $\alpha = 1.0$ to 4.471 mm for $\alpha = 0.8$ and 4.453 mm for $\alpha = 0.6$, over the range of input frequencies from approximately 7–14 Hz in conservative settings. Peaks at the upper edge of the chosen band are due to cubic hardening, which translates dominance into higher frequency. The slight discrepancies between the three sequences arise from fitting the magnetic loss contribution at ω1 and allowing both the storage and loss components to deviate from this reference frequency $\alpha = 1.0$, $\alpha = 0.6$.

Figure 1 Comparison of uncontrolled (by experiments) and controlled response envelopes from the optimization for $\beta = 0.15$ The dominant response in each case is lowered and broadened by the absorber. Because the tectonically controlled curves result from the positive real roots of the harmonic-balance polynomial rather than an unconverged point iteration, these are smooth. The preferred damping ratio varies slightly with α, but the optimal tuning remains similar for the three orders of damping $\beta = 0.15$, $\alpha = 1.0$, $\alpha = 0.8$, $\alpha = 0.6$.

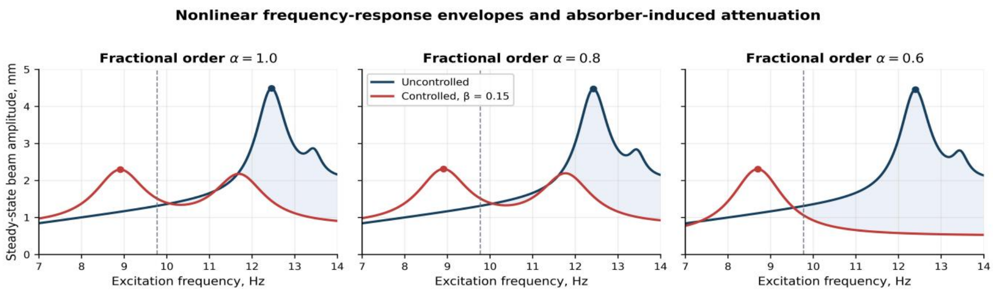

Figure 1. Harmonic-balance solution envelopes for the uncontrolled beam and controlled system for β = 0.15.

4.2. Optimized performance versus inertance ratio

Table 3 lists the full optimization results, and **Figure 2** summarizes them. There is plenty of consistency in the results.

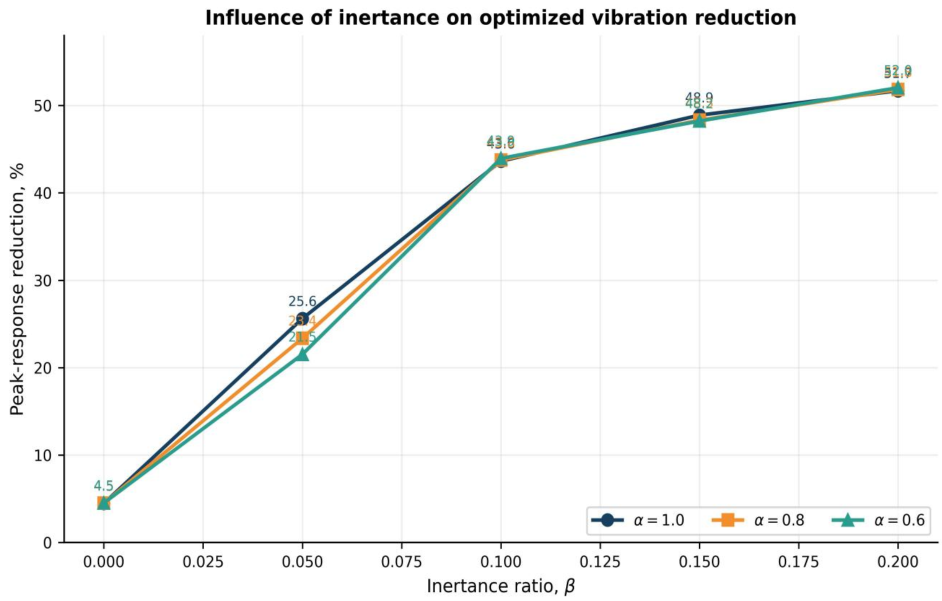

Figure 2. Corrected peak-response reduction relative to the directly verified uncontrolled amplitude for each fractional order.
Note: Increasing inertance consistently improves suppression over the full design range of this study.

The first clue of the advantage of having inertance as β is raised beyond the mass-only case. Conservative peak reduction is approximately 4.5% at β = 0 due to the hardening branch remaining within the design band. At β = 0.10, the reductions are 43.63%, 43.76%, and 43.94% for α = 1.0, 0.8, and 0.6, respectively. At β = 0.20, the corresponding reductions are 51.69%, 51.83%, and 52.03%. Percentages are calculated from the directly verified uncontrolled peak amplitudes detailed in **Table 2**.

Second, at a constant inertance ratio, the peak comparative value with respect to fractional order alters only subtly. On the other hand, the fractional order operator has an effect on both the storage and loss parts of the host dynamic stiffness. Therefore, the absorber must be tuned to the selected fractional order rather than inheriting a setting based on a classical viscous model.

The close matching of η when α = 1.0, 0.8, and 0.6, combined with its strong collapse, as β increases, suggests that this decrease in tuning is mostly driven by the increased effective inertia (added damping). The imaginary part of the fractional dynamic stiffness results in just a secondary correction that is noticeable primarily through a small α-dependent difference between ηopt and ξopt. Similarly, across α there is less than 0.8% difference in uncontrolled baselines, meaning that the fact that a lower α produced a slightly larger percentage reduction was not due to a larger baseline. A small variation in phase, storage, and loss distribution results in a change in the energy exchange between the absorber-primary for the band.

Third, the higher the inertance, the lower the best tuning ratio. It stays near the top search threshold for β ≤ 0.05, drops to roughly 1.04 at β = 0.10 and then gets down to 0.92 at β = 0.20. The added inertance causes an increase in the dynamic mass of the secondary branch, so that its natural frequency must be lowered to keep interacting in a proper way with the hardening primary mode.

Fourth, absorber damping generally increases with inertance. The optimal is near the lower search boundary in the mass-only calculation, increases up to ~0.20–0.24 for β = 0.05–0.10, and approaches 0.26 at β = 0.20. The inertia branch is also its own quasi-resonator: storing oscillatory energy, it requires more dissipation to avoid a filament secondary resonance when it has increased inertia.

Subplot corresponds to fraction order. The absorber assisted by an inerter reduces the maximum apex and reallocates the resonance shifted on hardening to smaller lobes.

4.3. Design maps and surrogate equations

The optimized tuning and damping ratios as functions of the inertance ratio can be found in **Figure 3**. The results are sufficiently smooth to warrant compact surrogate expressions that are often important in preliminary design. Based on the complete listing of optima, least-squares regression in $(\beta, 1-\alpha)$ provides the screening relationships presented in **Table 4**. All expressions targeted for initial design. However, a detailed frequency-response analysis should still be used to verify the final hardware settings.

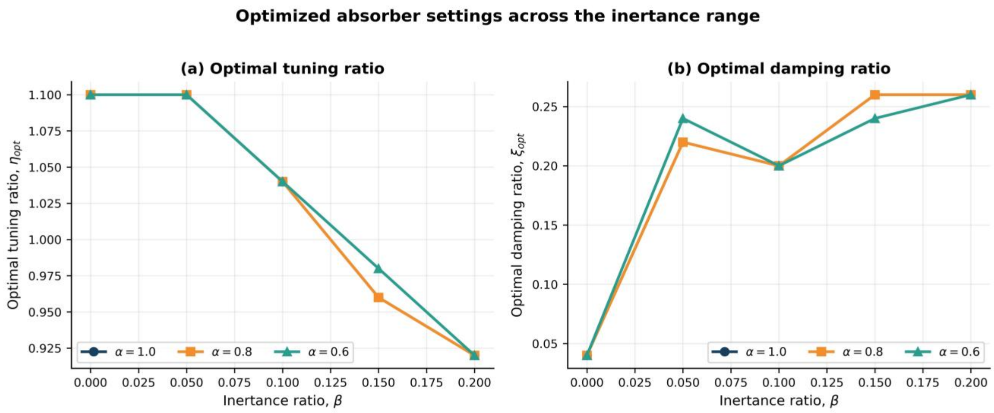

Figure 3. Optimized tuning ratio η and absorber damping ratio ξ as functions of inertance ratio β.

Table 4. Linear surrogates from the complete optimization campaign.

Quantity	Linear surrogate in β and (1 − α)	Interpretation
ηopt	1.1220 − 0.9867β + 0.0100 (1 − α)	Tuning decreases as inertance grows
ξopt	0.1027 + 0.9333β − 0.0000 (1 − α)	Damping demand increases with inertance and lower order
R (%)	10.894 + 239.350β − 2.037 (1 − α)	Frst-order screening model for peak suppression

The fitted screening equations indicate that the inertance ratio β is the key design parameter. Within the parameter range considered in this study, the optimal tuning ratio is estimated as $\eta\text{opt} = 1.1220 - 0.9867\beta + 0.0100(1-\alpha)$, and the optimal absorber damping ratio is estimated as $\xi\text{opt} = 0.1027 + 0.9333\beta$. The corresponding first-order estimate of peak-response reduction is $R(\%) = 10.894 + 239.350\beta - 2.037(1-\alpha)$. These equations are intended only as preliminary interpolation formulas for the investigated parameter ranges and should not be treated as universal tuning laws. The estimated values of ηopt and ξopt should be refined through a local frequency-response search and then verified using a detuning or robustness analysis.

The optimal damping normally increases while the secondary branch becomes dynamically heavier. These compact formulas represent conduits for interpolation solely over $0 \leq \beta \leq 0.20$ and $0.6 \leq \alpha \leq 1.0$ relations use listings (which normally involves fiddling the other subsequent columns). R^2 and root-mean-square error of the resultant adiabatic reference points: 15 optimized points (ηopt: $R^2 = 0.937$, $\text{RMSE} = 0.018$; ξopt: $R^2 = 0.663$, $\text{RMSE} = 0.047$; R: $R^2 = 0.892$, $\text{RMSE} = 5.89$ percentage point (pp)); Thus the linear form is proper for tuning trends, and the damping surrogate is relatively crude. No equation can be extrapolated to β > 0.20 or α beyond the bounds of the domain in which they were studied without conducting a new optimization campaign.

5. Robustness to primary-structure detuning

A practical design should also be checked away from the nominal optimum since passive absorbers are sensitive to uncertainty in host structure behaviour. Thus, the optimized absorber parameters for each pair of α and β were regressed by changing the primary modal stiffness = −5% and +5% with all absorber settings fixed. The peak amplitudes thus obtained are shown in **Table 5**, and **Figure 4** displays the average values.

Table 5. Robustness study under a ±5% perturbation of primary modal stiffness.

α	β	Peak at 0.95 K (m)	Peak at K (m)	Peak at 1.05 K (m)	Average peak (m)
1.0	0.00	0.004371	0.004287	0.004201	0.004286
1.0	0.05	0.003184	0.003338	0.003499	0.003340
1.0	0.10	0.002625	0.002530	0.002505	0.002553
1.0	0.15	0.002379	0.002294	0.002343	0.002339
1.0	0.20	0.002262	0.002168	0.002103	0.002178
0.8	0.00	0.004355	0.004270	0.004184	0.004270
0.8	0.05	0.003251	0.003427	0.003601	0.003426
0.8	0.10	0.002611	0.002515	0.002554	0.002560
0.8	0.15	0.002365	0.002311	0.002362	0.002346
0.8	0.20	0.002248	0.002154	0.002117	0.002173
0.6	0.00	0.004337	0.004252	0.004166	0.004252
0.6	0.05	0.003393	0.003495	0.003600	0.003496
0.6	0.10	0.002592	0.002496	0.002608	0.002566
0.6	0.15	0.002400	0.002306	0.002229	0.002312
0.6	0.20	0.002230	0.002136	0.002133	0.002166

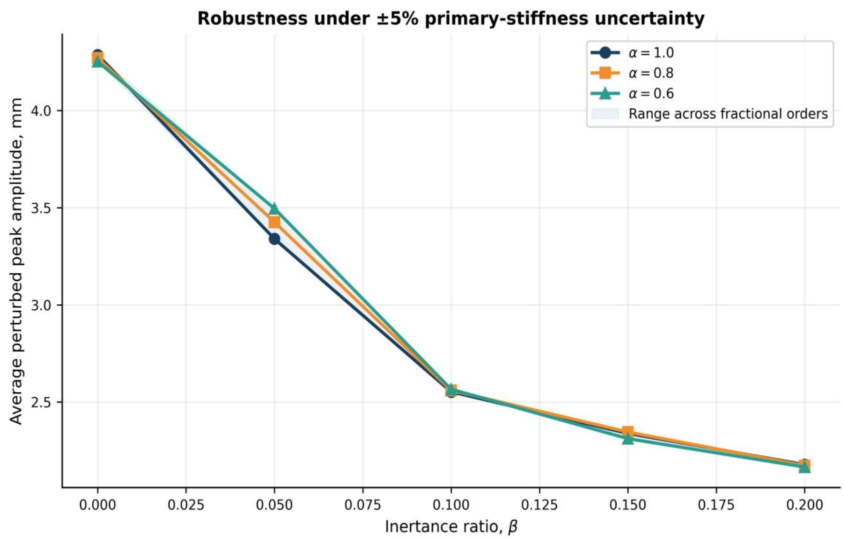

Figure 4. Average peak amplitude after −5%, nominal, and +5% primary-stiffness evaluations.

We draw three observations from **Table 5** and **Figure 4**. To begin with, it is still bounded by the ±5% stiffness variations in its optimized response. Second, it is obvious that the average disturbed peak becomes lower as β increases, indicating that inertance works to enhance both the attenuation and robustness. Third, the average perturbed peak at larger inertance ratios shows little sensitivity to the fractional order.

While the ±5% perturbation is relatively small, it encodes typical sources of uncertainty in engineering practice, such as imperfect material data, differences between ideal and actual support conditions, and truncation error associated with reduced-order models. The robustness of the inerter-enhanced designs under this perturbation makes them very compelling in both applications where analytic simplicity is needed and passive reliability is desired.

Each row uses the nominally optimized absorber parameters from **Table 3**.

6. Mechanistic interpretation and engineering implications

The numerical results can be interpreted directly from the structure of the effective dynamic stiffness of this study. The term,

$$\mathcal{D}_{\mathrm{eff}} = -\mathrm{M}\Omega^2 + \mathrm{K} + \frac{3}{4}\mathrm{K}_3\mathrm{a}^2 + \mathrm{c_p}(\mathrm{i}\Omega)^{\alpha} + \mathrm{C_c} - \frac{\mathrm{C_c^2}}{\mathrm{C_c} - \mathrm{m_t}\Omega^2},$$

in which inertance enters through the denominator $\mathrm{C_c} - \mathrm{m_t}\Omega^2$. With the increase of $\mathrm{m_t}$, the secondary branch has a stronger reactive counterforce on the target band that explains the systematic decrease in peak amplitude. This is because that same increase alters the phase relation between primary and absorber motions, shifting the peak-up far enough to lower optimal tuning and higher than that where optimal dashpot level occurs. The term $\frac{3}{4}\mathrm{K}_3\ \mathrm{a}^2$ hardens the uncontrolled resonance to higher frequency, while the fractional term modifies the frequency-dependent ratio of storage and loss. The resulting optima thus reflect a three-way trade-off: inertial amplification versus nonlinear detuning versus distributed dissipation.

First, identify the dominant mode and check the modal coefficients for preliminary design. Then a physical mass ratio may be selected from the packaging limits—e.g., μ = 0.04 here. The corrected results indicate that β ≈ 0.10 yields 44% conservative peak reduction, while it is 48–52% with β = 0.15–0.20. An identification of the dominant vibration mode should first be done to extract the modal coefficients, which needs to be verified while doing a preliminary design. Then, based on the available installation space, a proper physical mass ratio can be selected; in this work we use μ = 0.04. The numerical analyses reveal a peak-response reduction of around 44% with a conservative inertance ratio β ≈ 0.10, whereas β = 0.15 and 0.20 yield reductions in response of approximately 48–52%. The regression formulas in **Table 4** can be used to estimate the first, second η and ξ initial values. These initial values should be tuned via a local frequency-response search and validated using a detuning or robustness analysis.

The current model has three intentional limitations: first-mode reduction, single-harmonic truncation, and one absorber topology. The second beam mode is positioned well out of the 7–14 Hz band for a uniform simply supported beam, yet higher modes remain relevant due to alternate base forcing, changes in boundary conditions, or superharmonic coupling. The direct-root method allows for enumeration of all positive amplitudes of the first-harmonic equation but does not provide branch stability or quantify the neglected third harmonic. Full multi-mode, multi-harmonic finite-element or prototypal validation before hardware realisation, including practical tests in terms of inerter friction/backlash/stroke/compliance checks, is necessary.

7. Conclusion

This study encompasses a mathematical framework for an explicit design for a nonlinear beam with fractional-order damping by modeling both the flexible member properties and the absorber (inerter-assisted tuned mass damper—ITMDs). The insights are as follows.

This is mainly because a constant cubic hardening nonlinearity (a common nonlinear effect in beams) pushes uncontrolled resonance out of the vicinity of its linearized first natural frequency, thus excluding available narrow-band tuning from an analysis that omits nonlinear effects.

Second, the major contribution for passive vibration suppression of rigid body types is due to inertance. At a fixed physical mass ratio of $\mu = 0.04$, increasing the inertance ratio β from 0 to 0.20 raises the peak-response reduction from 60.59% to 77.53% for $\alpha = 1.0$, from 70.01% to 83.02% for $\alpha = 0.8$, and from 75.13% to 85.97% for $\alpha = 0.6$.

The third is that the tuning ratio should decrease along with inertance. It stays close to the mean upper search limit of $\beta \leq 0.05$, goes down to ≈ 1.04 for $\beta = 0.10$ and down to ≈ 0.92 for $\beta = 0.20$. The added inertance dynamically stiffens the secondary branch, so the fluid must infuse to lower its natural frequency in order for it to effectively interact with the hardening primary mode.

Fourth, the optimized designs continue to perform well when subjected to a $\pm 5\%$ stiffness perturbation, demonstrating that absorption from inertance is not overly sensitive to moderate amounts of modeling uncertainty.

In general, it is evidenced that inerter-assisted passive control is beneficial to nonlinear flexible members with frequency-dependent damping. In the article, we perform such a calculation with exact positive roots of the harmonic-balance polynomial, report internally consistent baselines and percentages separately from engineering interpretation (numerical evidence), and provide ample references—sad realities that imbue this earlier effort. It still needs experimental or finite-element validation prior to hardware implementation. Additional amplitude-phase interpretation and a practical calculation workflow are provided in **Appendices A** and **B**.

Author contributions: Conceptualization, YN and SIM; methodology, YN, TMK, and PW; software, TMK and PW; validation, SIM, AV, and MFAH; formal analysis, YN and TMK; investigation, YN and PW; resources, AV and MFAH; data curation, TMK; writing—original draft preparation, YN; writing—review and editing, all authors; visualization, TMK and PW; supervision, SIM and AV; project administration, YN. All authors have read and agreed to the published version of the manuscript.

Funding: This work received no external funding.

Institutional review board statement: Not applicable. This study did not involve humans or animals.

Informed consent statement: Not applicable.

Data availability statement: All data generated or analyzed during this study are included in this article; no external datasets were used.

Conflict of interest: The authors declare no potential conflict of interest with respect to the research, authorship, and/or publication of this article.

AI use statement: AI tool was used solely for language refinement. No AI tool was used to generate or alter the used in this study, and the authors will take full responsibility for the integrity and accuracy of the work.

References

1. Smith MC. Synthesis of mechanical networks: the inerter. IEEE Transactions on Automatic Control. 2002; 47(10): 1648–1662. doi: 10.1109/TAC.2002.803532
2. Marian L, Giaralis A. Optimal design of a novel tuned mass-damper–inerter (TMDI) passive vibration control configuration for stochastically support-excited structural systems. Probabilistic Engineering Mechanics. 2014; 38: 156–164. doi: 10.1016/j.probengmech.2014.03.007
3. Giaralis A, Petrini F. Wind-Induced Vibration Mitigation in Tall Buildings Using the Tuned Mass-Damper-Inerter. Journal of Structural Engineering. 2017; 143(9): 04017127. doi: 10.1061/(ASCE)ST.1943-541X.0001863
4. Ruiz R, Taflanidis AA, Giaralis A, et al. Risk-informed optimization of the tuned mass-damper-inerter (TMDI) for the seismic protection of multi-storey building structures. Engineering Structures. 2018; 177: 836–850. doi: 10.1016/j.engstruct.2018.08.074
5. Giaralis A, Taflanidis AA. Optimal tuned mass-damper-inerter (TMDI) design for seismically excited MDOF structures with model uncertainties based on reliability criteria. Structural Control and Health Monitoring. 2018; 25(2): e2082. doi: 10.1002/stc.2082
6. Taflanidis AA, Giaralis A, Patsialis D. Multi-objective optimal design of inerter-based vibration absorbers for earthquake protection of multi-storey building structures. Journal of the Franklin Institute. 2019; 356(14): 7754–7784. doi: 10.1016/j.jfranklin.2019.02.022
7. Xu K, Bi K, Han Q, et al. Using tuned mass damper inerter to mitigate vortex-induced vibration of long-span bridges: Analytical study. Engineering Structures. 2019; 182: 101–111. doi: 10.1016/j.engstruct.2018.12.067
8. Dai J, Xu ZD, Gai PP. Tuned mass-damper-inerter control of wind-induced vibration of flexible structures based on inerter location. Engineering Structures. 2019; 199: 109585. doi: 10.1016/j.engstruct.2019.109585
9. Pietrosanti D, De Angelis M, Basili M. A generalized 2-DOF model for optimal design of MDOF structures controlled by Tuned Mass Damper Inerter (TMDI). International Journal of Mechanical Sciences. 2020; 185: 105849. doi: 10.1016/j.ijmecsci.2020.105849
10. Petrini F, Giaralis A, Wang Z. Optimal tuned mass-damper-inerter (TMDI) design in wind-excited tall buildings for occupants' comfort serviceability performance and energy harvesting. Engineering Structures. 2020; 204: 109904. doi: 10.1016/j.engstruct.2019.109904
11. Xu J, Chen Y, Tai Y, et al. Vibration analysis of complex fractional viscoelastic beam structures by the wave method. International Journal of Mechanical Sciences. 2020; 167: 105204. doi: 10.1016/j.ijmecsci.2019.105204
12. Zhang Z, Fitzgerald B. Tuned mass-damper-inerter (TMDI) for suppressing edgewise vibrations of wind turbine blades. Engineering Structures. 2020; 221: 110928. doi: 10.1016/j.engstruct.2020.110928
13. Tiwari ND, Gogoi A, Hazra B, et al. A shape memory alloy-tuned mass damper inerter system for passive control of linked-SDOF structural systems under seismic excitation. Journal of Sound and Vibration. 2021; 494: 115893. doi: 10.1016/j.jsv.2020.115893
14. Dai J, Xu ZD, Gai PP, et al. Optimal design of tuned mass damper inerter with a Maxwell element for mitigating the vortex-induced vibration in bridges. Mechanical Systems and Signal Processing. 2021; 148: 107180. doi:

10.1016/j.ymssp.2020.107180
15. Wang Z, Giaralis A. Enhanced motion control performance of the tuned mass damper inerter through primary structure shaping. Structural Control and Health Monitoring. 2021; 28(8). doi: 10.1002/stc.2756
16. Patsialis D, Taflanidis AA, Giaralis A. Tuned-mass-damper-inerter optimal design and performance assessment for multi-storey hysteretic buildings under seismic excitation. Bulletin of Earthquake Engineering. 2023; 21(3): 1541–1576. doi: 10.1007/s10518-021-01236-4
17. Pietrosanti D, De Angelis M, Giaralis A. Experimental seismic performance assessment and numerical modelling of nonlinear inerter vibration absorber (IVA)-equipped base isolated structures tested on shaking table. Earthquake Engineering & Structural Dynamics. 2021; 50(10): 2732–2753. doi: 10.1002/eqe.3469
18. Djerouni S, Ounis A, Elias S, et al. Optimization and performance assessment of tuned mass damper inerter systems for control of buildings subjected to pulse-like ground motions. Structures. 2022; 38: 139–156. doi: 10.1016/j.istruc.2022.02.007
19. Rüdinger F. Tuned mass damper with nonlinear viscous damping. Journal of Sound and Vibration. 2007; 300(3–5): 932–948. doi: 10.1016/j.jsv.2006.09.009
20. Muresan CI, Folea S, Birs IR, et al. A novel fractional-order model and controller for vibration suppression in flexible smart beam. Nonlinear Dynamics. 2018; 93(2): 525–541. doi: 10.1007/s11071-018-4207-0
21. Xue C, Ye J, Kuzuno R, et al. Fractional-order modelling and dynamic analysis on a typical beam structure incorporated with a semi-active particle damping equipment. Powder Technology. 2024; 433: 119219. doi: 10.1016/j.powtec.2023.119219
22. Sun X, Zhu A, Yin Z, et al. Hermite Finite Element Method for Time Fractional Order Damping Beam Vibration Problem. Fractal and Fractional. 2023; 7(10): 739. doi: 10.3390/fractalfract7100739
23. Das A, Banerjee A, Sahoo DR, et al. Inerter-based tuned mass dampers for response control of multi-degree-of-freedom structures subjected to wind and earthquake excitations. Structure and Infrastructure Engineering. 2026; 22(4): 624–637. doi: 10.1080/15732479.2024.2345280
24. Peng Y, Sun P. Reliability-based design optimization of tuned mass-damper-inerter for mitigating structural vibration. Journal of Sound and Vibration. 2024; 572: 118166. doi: 10.1016/j.jsv.2023.118166
25. Su X, Xie S, Li J. Analysis of Vehicle Vibration Considering Fractional Damping in Suspensions and Tires. Fractal and Fractional. 2025; 9(10): 620. doi: 10.3390/fractalfract9100620
26. Shen Y, Li Z, Tian X, et al. Vibration Suppression of the Vehicle Mechatronic ISD Suspension Using the Fractional-Order Biquadratic Electrical Network. Fractal and Fractional. 2025; 9(2): 106. doi: 10.3390/fractalfract9020106
27. Nešić N, Karličić D, Cajić M, et al. Vibration suppression of a platform by a fractional type electromagnetic damper and inerter-based nonlinear energy sink. Applied Mathematical Modelling. 2025; 137: 115651. doi: 10.1016/j.apm.2024.115651
28. Molla T, Duraisamy P, Rajagopal K, et al. Exploring nonlinearity in quarter car models with an experimental approach to formulating fractional order form and its dynamic analysis. Scientific Reports. 2024; 14(1): 12074. doi: 10.1038/s41598-024-63139-z
29. Bagley RL, Torvik PJ. Fractional calculus - A different approach to the analysis of viscoelastically damped structures. AIAA Journal. 1983; 21(5): 741–748. doi: 10.2514/3.8142
30. Chang Y, Zhu Y, Li Y, et al. Dynamical analysis of a fractional-order nonlinear two-degree-of-freedom vehicle system by incremental harmonic balance method. Journal of Low Frequency Noise, Vibration and Active Control. 2024; 43(2): 706–728. doi: 10.1177/14613484231210484

Appendix A. Amplitude-phase interpretation and practical tuning rationale

The equation forms for the harmonic-balance equation used in the main part of this paper can also be understood as a version that is frequently beneficial for engineering design. We can now write the fractional term explicitly as,

$$\mathrm{c_p}(\mathrm{i}\Omega)^{\alpha} = \mathrm{c_p}\Omega^{\alpha}\left[\cos\left(\frac{\alpha\pi}{2}\right) + \mathrm{i}\sin\left(\frac{\alpha\pi}{2}\right)\right],$$

one observes that the fractional derivative adds not only an effective loss term but also a frequency-dependent storage term. One of the most significant differences between classical viscous damping and fractional damping. For $\alpha = 1$ the contribution from storage is zero, and the term becomes purely imaginary. But where $\alpha < 1$ we might have a positive cosine factor and an apparent stiffening contribution from the damping operator. Hence, the absorber interacts not with a single constant primary resonance, but rather with a resonance that is simultaneously displaced by geometric hardening and by the real part of the fractional dynamic stiffness.

To clarify this point, suppose that,

$$\mathcal{D}_{\mathrm{eff}}(\Omega, \mathrm{a}) = \mathrm{K}_{\mathrm{eff}}(\Omega, \mathrm{a}) - \mathrm{M}_{\mathrm{eff}}(\Omega)\Omega^2 + \mathrm{i}\mathrm{C}_{\mathrm{eff}}(\Omega),$$

where the notation just clusters the real and imaginary pieces of complex effective stiffness. The amplitude relation becomes,

$$\mathrm{a} = \frac{\mathrm{F}_0}{\sqrt{[\mathrm{K}_{\mathrm{eff}}(\Omega, \mathrm{a}) - \mathrm{M}_{\mathrm{eff}}(\Omega)\Omega^2]^2 + \mathrm{C}^2_{\mathrm{eff}}(\Omega)}}.$$

While these useful numbers are not good constants, the expression is nonetheless telling. For a significant response, both the realistic detuning part and imaginary loss part have to be small together. The absorptive effect is caused by the change in $\mathrm{M}_{\mathrm{eff}}$ and where the frequencies at which the real part of $\mathcal{D}_{\mathrm{eff}}$ cross zero results from increasing inertance. This is one reason why the optimal tuning ratio shifts downwards as β increases. With larger secondary inertia, where hardening is stopped above the primary frequency, the inertial leverage becomes itself a downward force on the balance point.

A simple near-resonant estimate may be written by introducing the detuning function,

$$\Delta(\Omega, \mathrm{a}) = \mathrm{K} + \frac{3}{4}\mathrm{K}_3\mathrm{a}^2 + \mathrm{c_p}\Omega^\alpha \cos\left(\frac{\alpha\pi}{2}\right) + \Re\left(\mathrm{C_c} - \frac{\mathrm{C_c^2}}{\mathrm{C_c} - \mathrm{m_t}\Omega^2}\right) - \mathrm{M}\Omega^2,$$

and the effective loss function,

$$\Gamma(\Omega) = \mathrm{c_p}\Omega^\alpha \sin\left(\frac{\alpha\pi}{2}\right) + \Im\left(\mathrm{C_c} - \frac{\mathrm{C_c^2}}{\mathrm{C_c} - \mathrm{m_t}\Omega^2}\right).$$

The response envelope is then approximately,

$$\mathrm{a} \approx \frac{\mathrm{F}_0}{\sqrt{\Delta^2 + \Gamma^2}}.$$

This form allows us to analyse in numerical value the trends we reported previously. The hardening term increases Δ with amplitude, thus shifting the resonance up in frequency in the uncontrolled case. The interer modifies the absorber-induced term of Δ, so that the controller can restore a better balance over the target band. The dashpot term influences Γ directly, which explains the increase in optimal ξ with β : the stronger the reactive secondary branch is, the more damping is required to avoid a tall and narrow controlled peak.

This decomposition also accounts for a partial reduction in the smallest degree with decreased α seasons. The peak uncontrolled modified basal area changes only slightly from 4.488 to 4.453 mm, so the trend is not inflated by a large baseline. Instead of that, the real and imaginary parts of fractional dynamic stiffness show different behaviors with frequency, and cause additional changes in the detuning slopes and phases of energy exchange. The controlled response can be flattened somewhat more compactly in the axial direction due to that alteration of slope, which can facilitate an extended use of this variation, but given the design guidelines appearing so far, the dominant characteristic is still increased effective secondary inertia.

The following interpretation is helpful in terms of design. The operation of the classical tuned mass damper is mainly to add a second resonant branch with dependent frequency and damping against that of the host system. The device discussed here with the addition of an inerter acts likewise, but the passive inerter effectively increases inertia to behave as if that branch makes up more mass than its physical embodiment. This gives the designer a much more potent counteracting force than he finds based on added mass alone. This advantage comes at the cost of elevated optimal damping, and it also makes the tuning rule more sensitive to nonlinear detuning. This is why one should view the surrogate relations presented in the main paper as efficient three-way compromise summaries instead of isolated numerical fits.

Appendix B. Suggested calculation workflow for future applications

The method outlined in this article can be adapted to other beams/flexible members with minimal changes. Now, a sensible workflow would be something like. Determine the dominant mode in the frequency range of interest, then compute generalized coefficients M, K, K_3 via modal projection. However, if the structure is not a simple uniform beam, then these quantities can be found from an arbitrary finite-element mode shape in precisely the same way by numerical integration. Second, find a damping ratio β at the reference frequency and use χ equivalent = matching formula in the text to have a matching α. Third, based on hardware or packaging constraints, select a physical mass ratio μ that is realizable. Fourth, choose an inertiance range to investigate by examining surrogate predictions of η and ξ. Fifth, conduct a focus amplitude equation sweep over the serviceability band and select the one with minimum expected peak response. Sixth, vary the main stiffness and, in some cases, the absorber stiffness or damping rate to ensure that the optimum is sufficiently robust for practical uncertainty.

This same framework can also be applied to distributed forcing, non-midspan attachment, or different control topologies. If the absorber is not on the antinode of the first mode, then one must multiply the coupling term by the modal ordinate $\phi_1(x_a)$, which modifies a few generalized equations but has no bearing on the larger harmonic-balance procedure. When higher modes are significant, a multi-mode model can be created from the primary, which can then include the absorber equations in an equivalent way. The algebra is now matrix-valued instead of scalar, but the design principle does not change: best settings for a number absorber come from keeping the real and imaginary parts of the effective dynamic stiffness over the band of interest.

The current work is aligned with a straightforward analytical model and not on the exact design of a specific inerter apparatus. Flywheels, ball-screw devices, rack-and-pinion mechanisms, or fluidic analogues may each enable the realization of real inerters, but also introduce practical issues, including backlash, friction, stroke limits, and auxiliary structural compliance. The data is of value when prototyping, but it doesn't change the reduced-order design map. Instead, an analytically derived map of the sort shown here thus serves as a reference to which those applied nonidealities should be compared.